Supporting Information

Efficient electrochemical reduction of CO_2 promoted by the electrospun $Cu_{1.96}S$/Cu tandem catalyst

Shuo Liu, Yu Cao, Hai Liu, Huili Wang, Baoshan Zhang, Yiming Zhang, Lihong Zhang*, Sheng Zhang*, Jie Sun*

Key Laboratory for Green Chemical Technology of Ministry of Education, School of Chemical Engineering and Technology, Tianjin University, Tianjin, 300072, P.R. China

*Corresponding authors:
E-mail addresses: zlh_224@163.com (Lihong Zhang)
E-mail addresses: Sheng.zhang@tju.edu.cn (Sheng Zhang)
E-mail addresses: jies@tju.edu.cn (Jie Sun)

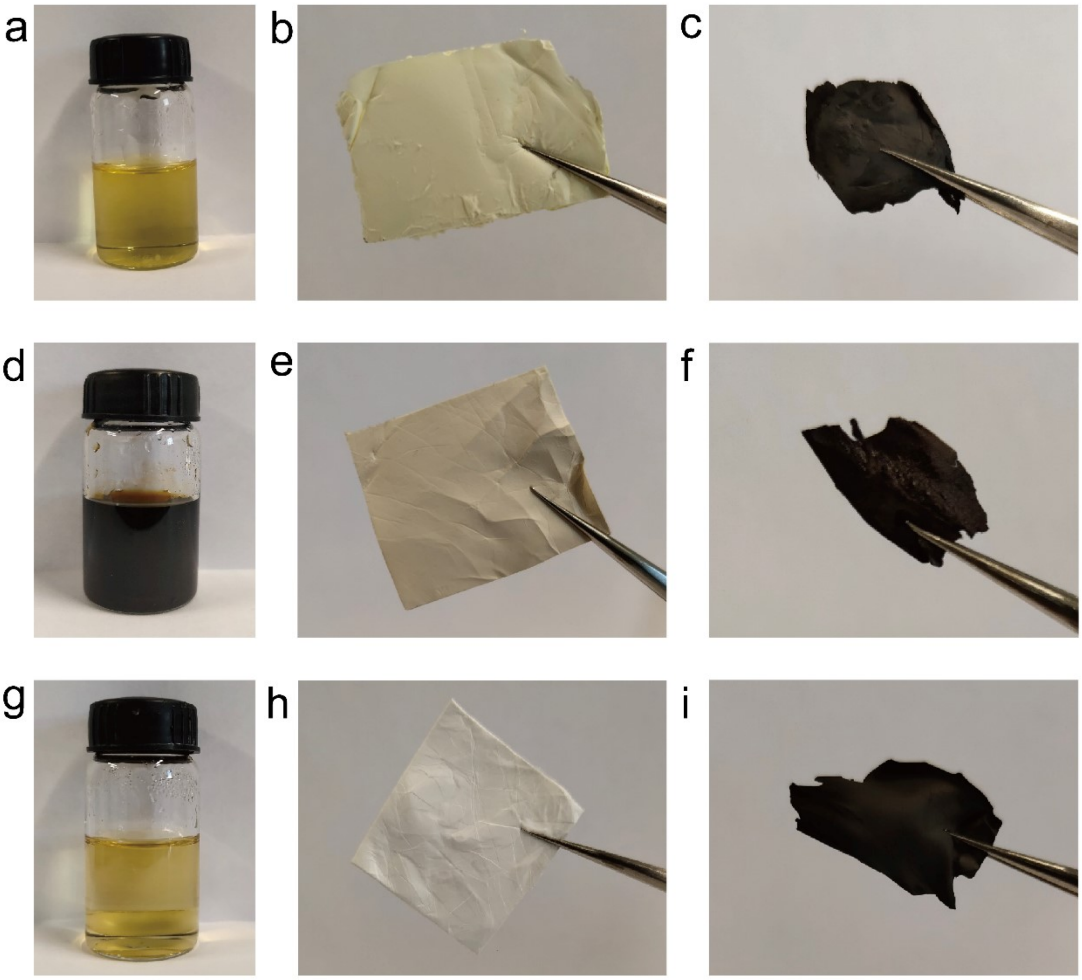

Fig. S1. Digital images of (a) electrospinning solution, (b) as spun nanofibers, (c) calcinated nanofibers of $Cu_{1.96}S$/Cu-NCNF. Digital images of (d) electrospinning solution, (e) as spun nanofibers, (f) calcinated nanofibers of Cu-NCNF. Digital images of (g) electrospinning solution, (h) as spun nanofibers, (i) calcinated nanofibers of NCNF.

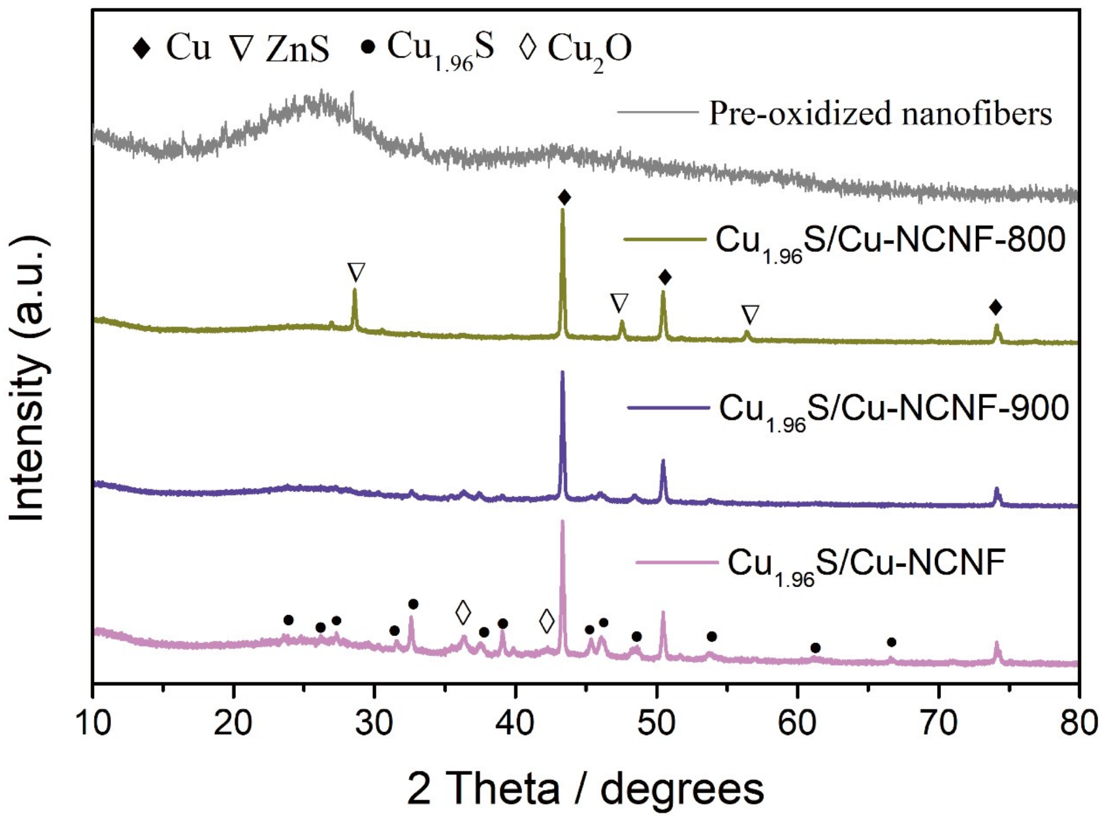

Fig. S2. XRD patterns of calcination of as-collected nanofibers at different temperatures. For pre-oxidized nanofibers, the weak peaks at 28.5°, 47.5° and 56.3°, relating to the (111), (220) and (311) planes of hexagonal ZnS crystalline phase (JCPDS No.36-1450), and the other composition is amorphous. For $Cu_{1.96}S$/Cu-NCNF-800, only the peaks of Cu and ZnS are observed, while the peaks of ZnS are increasing in intensity. For $Cu_{1.96}S$/Cu-NCNF-900, the phase transition from zinc sulfide to copper sulfide occurred.

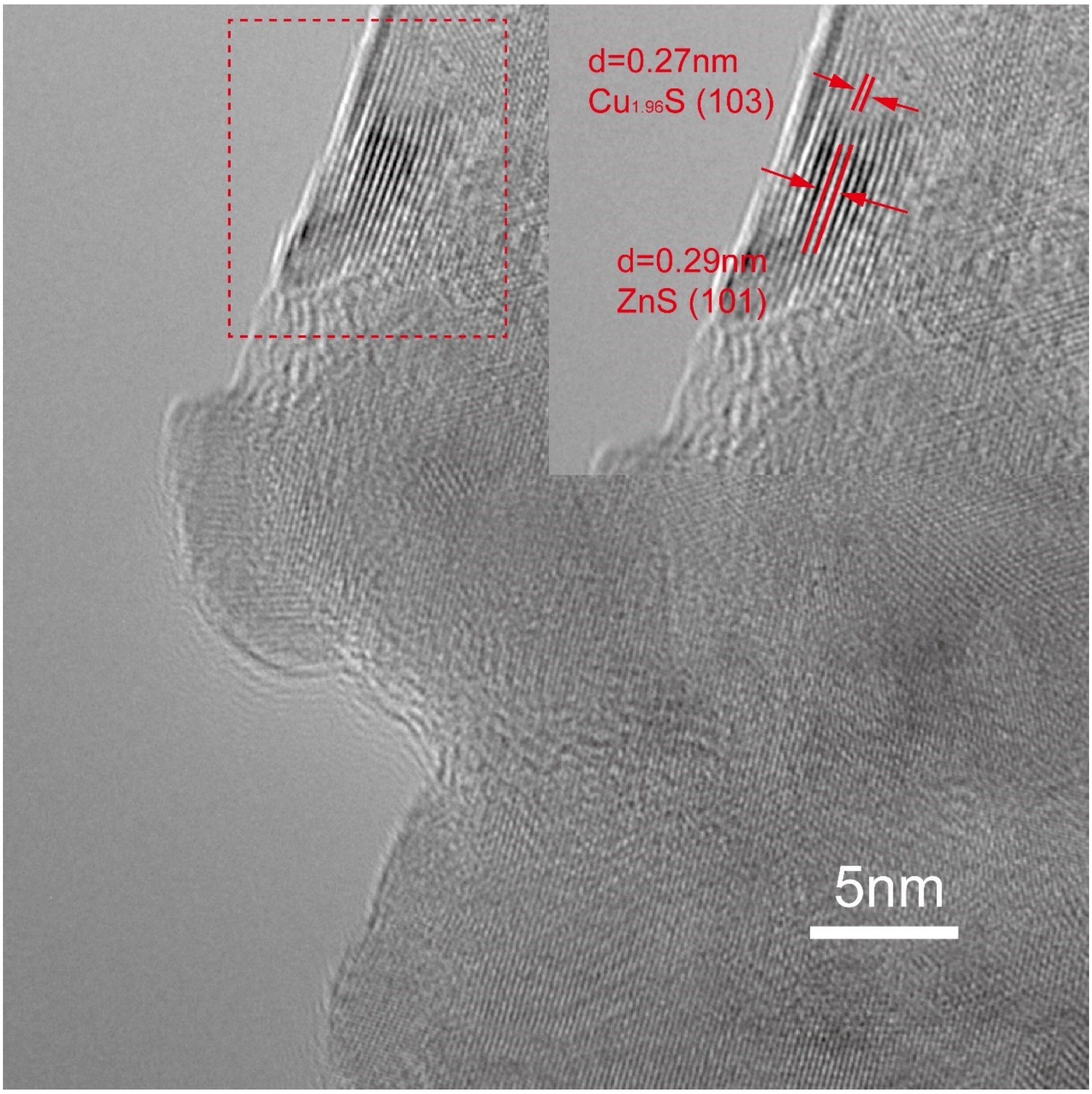

Fig. S3. HR-TEM image of $Cu_{1.96}S$/Cu-NCNF-900.

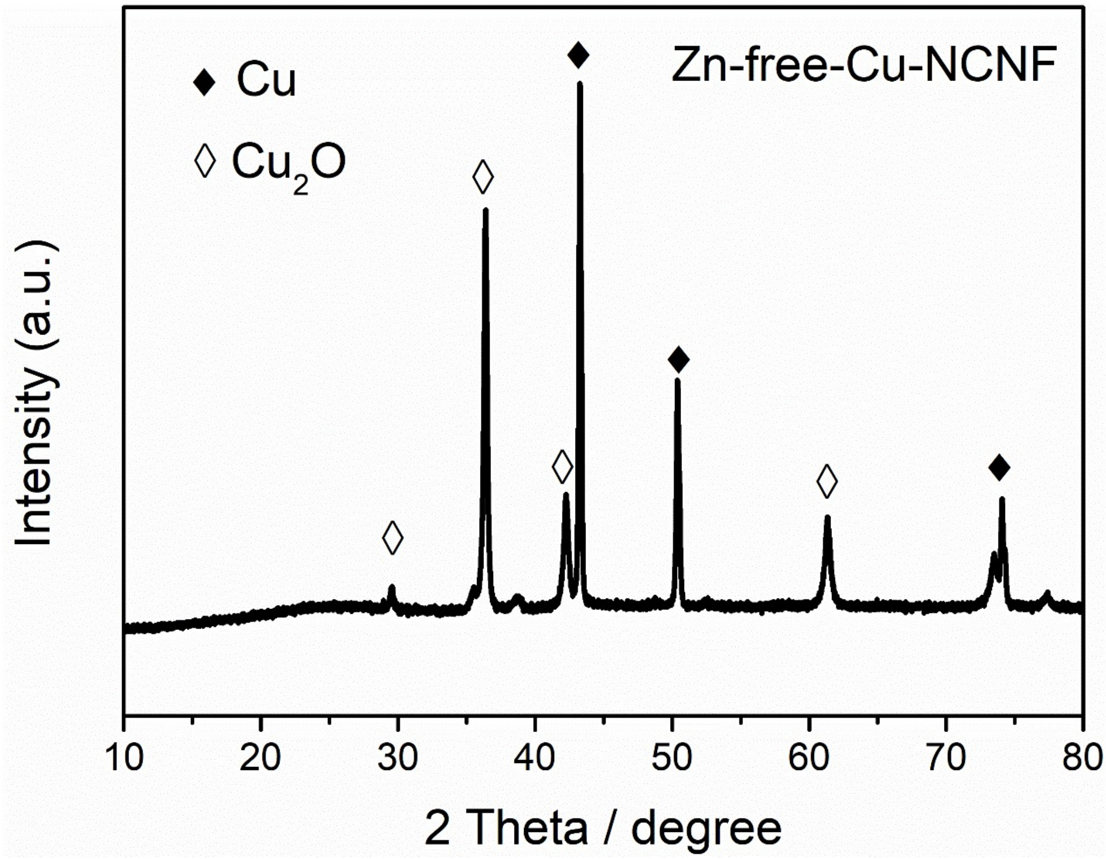

Fig. S4. XRD pattern of Zn-free-Cu-NCNF. The peaks at 29.6°, 36.4°, 42.3°, and 61.4° are consistent with cubic Cu_2O (JCPDS No. 78-2076).

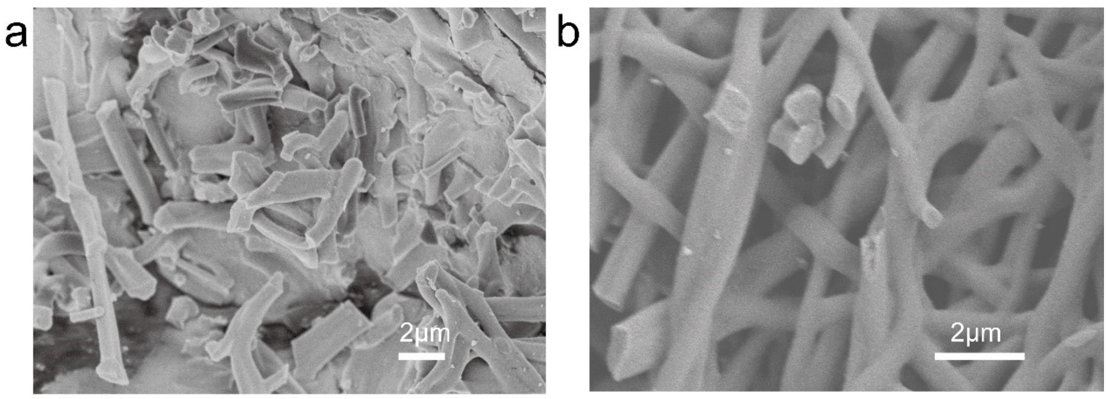

Fig. S5. SEM images of (a) Cu-NCNF and (b) NCNF

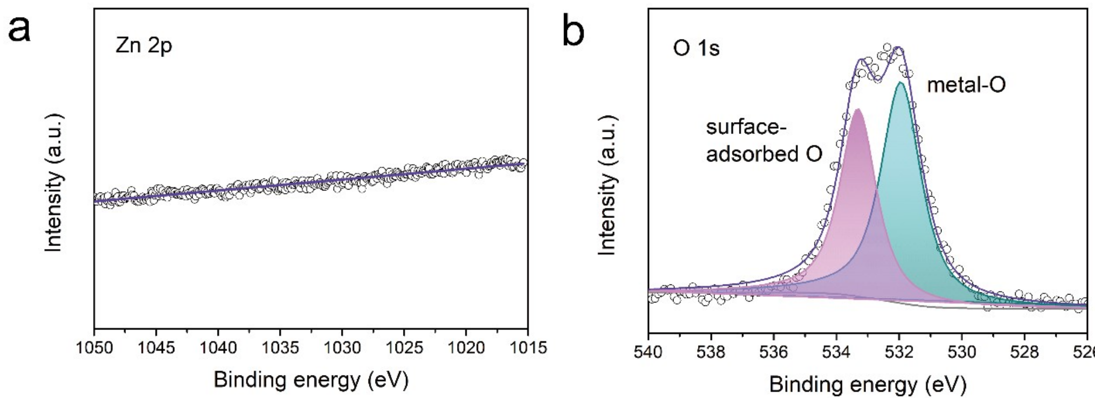

Fig. S6. High-resolution (a) Zn 2p, and (b) O 1s XPS spectra of $Cu_{1.96}S$/Cu-NCNF.

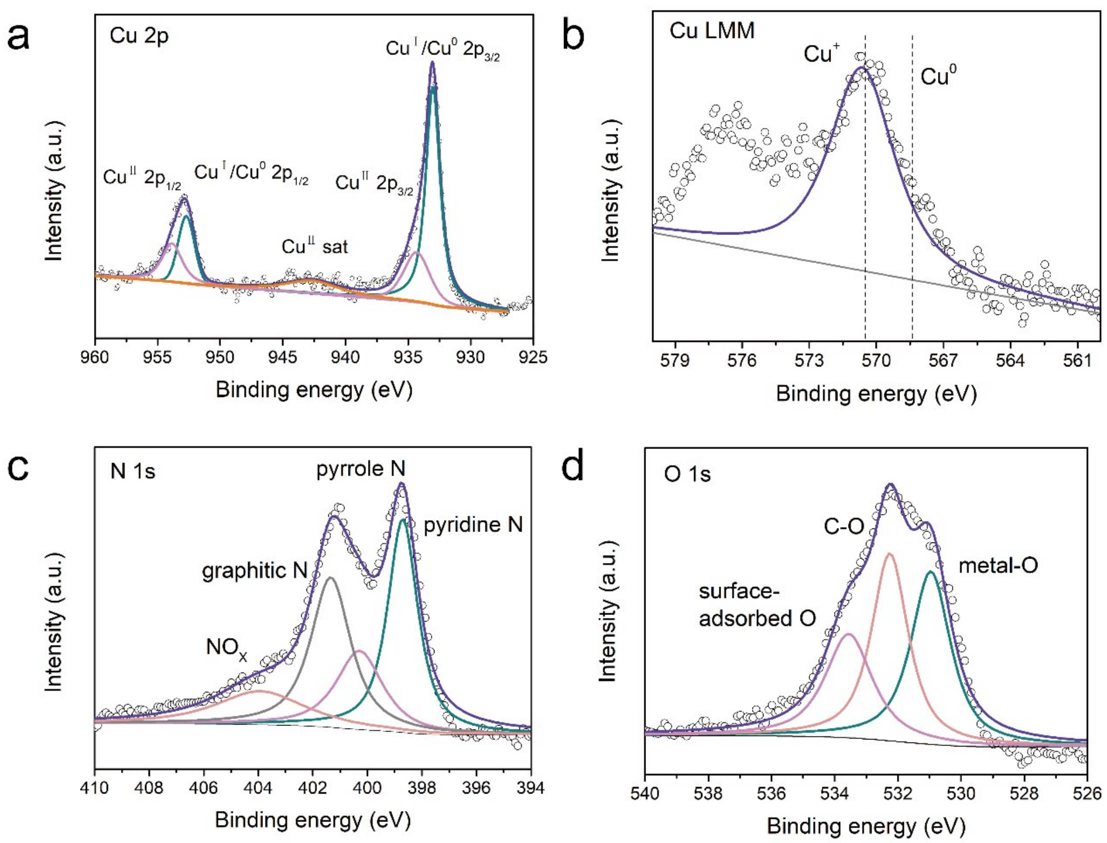

Fig. S7. High-resolution (a) Cu 2p, (b) Cu LMM, (c) N 1s, and (b) O 1s XPS spectra of Cu-NCNF.

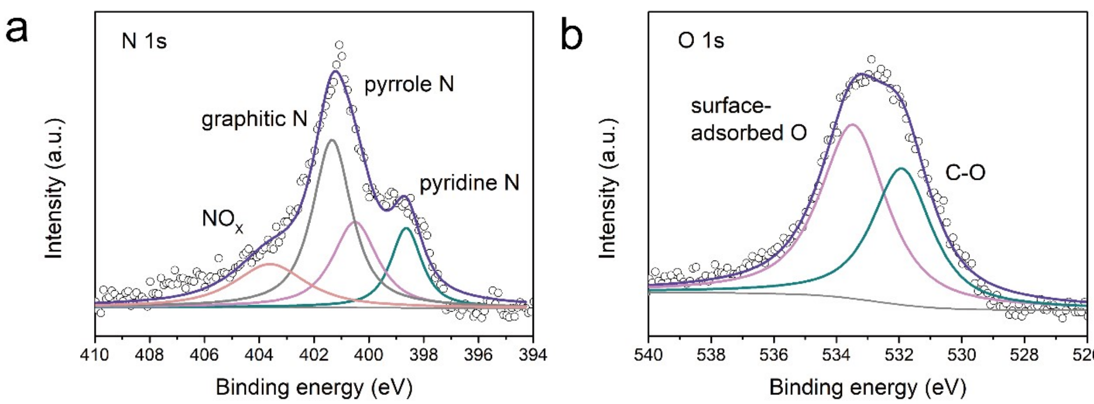

Fig. S8. High-resolution (a) N 1s, and (b) O 1s XPS spectra of NCNF.

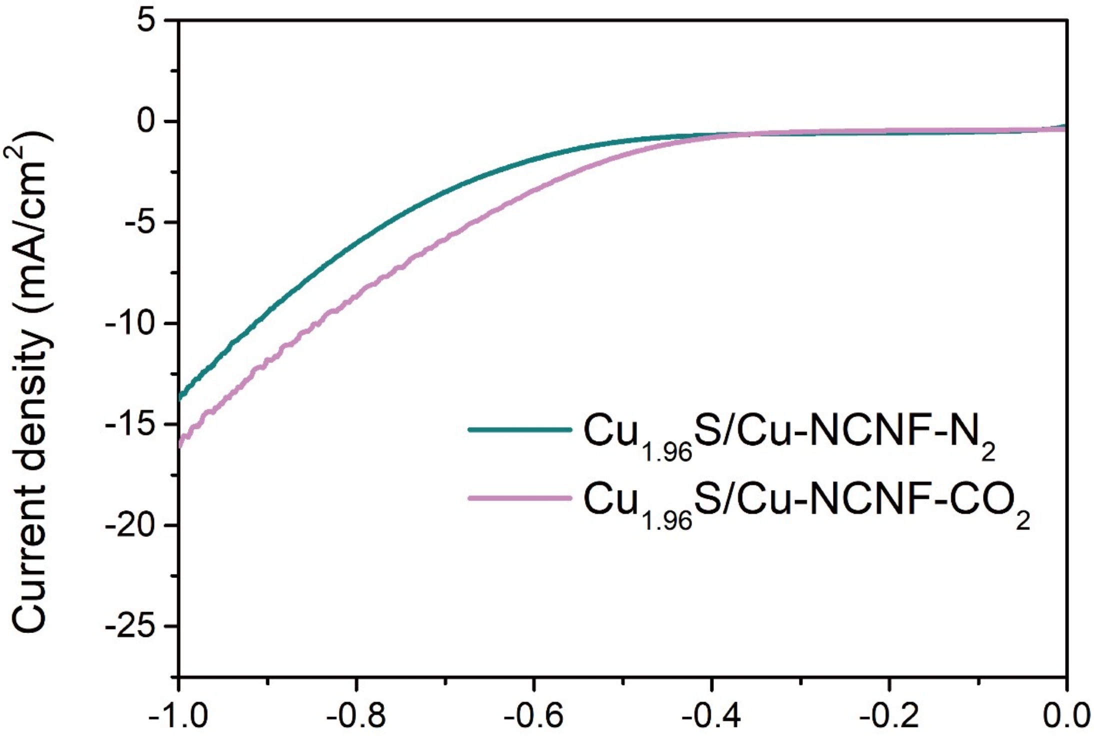

Fig. S9. LSV curves measured on $Cu_{1.96}S$/Cu-NCNF in N_2-and CO_2-saturated 0.5 M $KHCO_3$ aqueous solution with a scan rate of 5 mV s^{-1}.

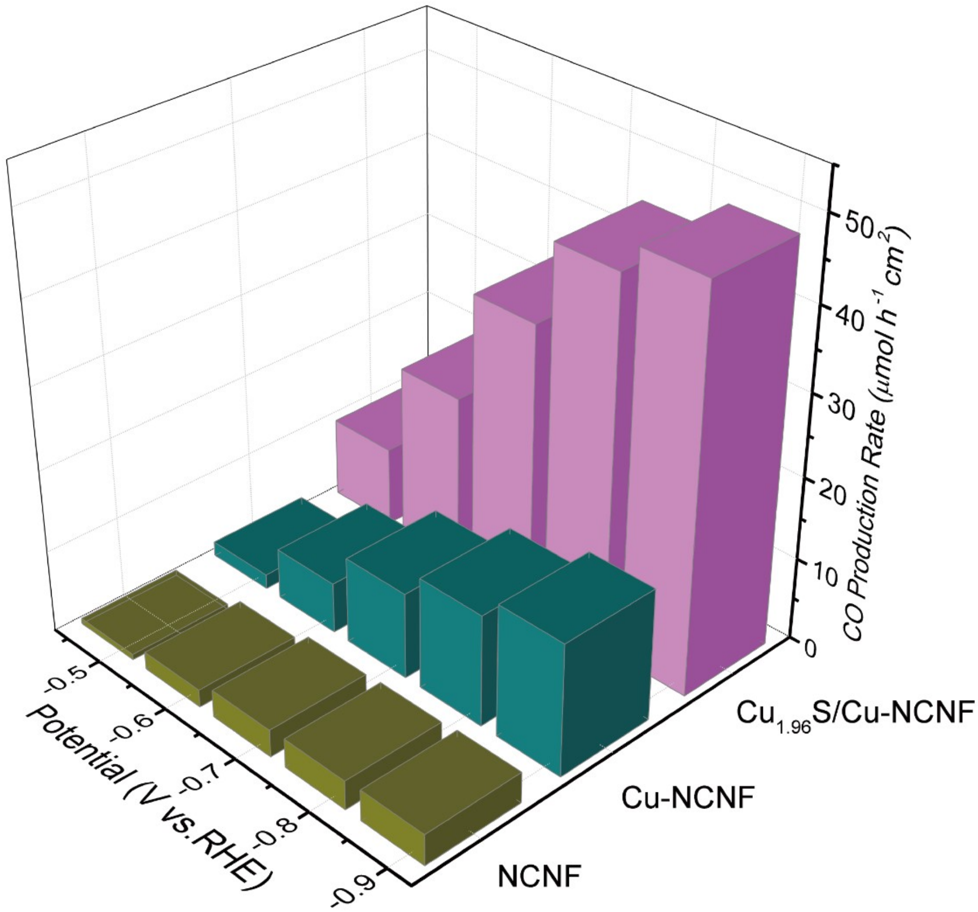

Fig. S10. CO production rate of $Cu_{1.96}S$/Cu-NCNF, Cu-NCNF and NCNF.

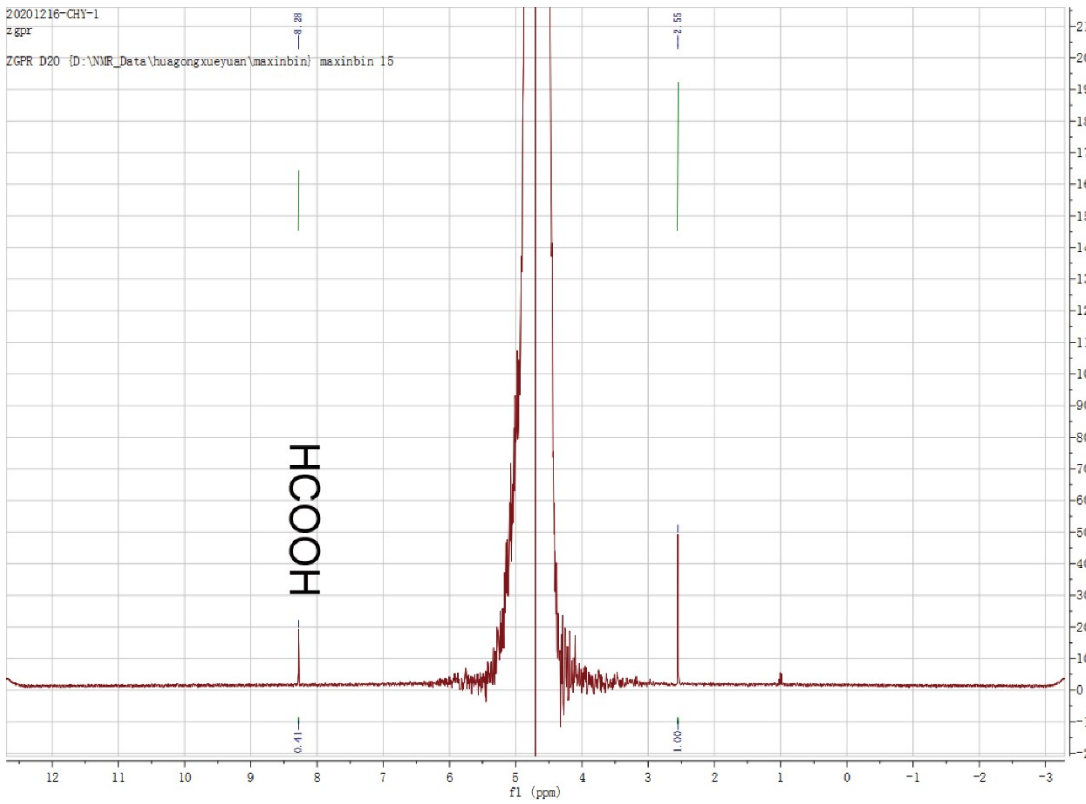

Fig. S11. ^{1}H NMR spectra of liquid products for CO_2RR at -0.68 vs. RHE over $Cu_{1.96}S$/Cu-NCNF. Only HCOOH is found as the liquid product and FE_{HCOOH} is about 8%.

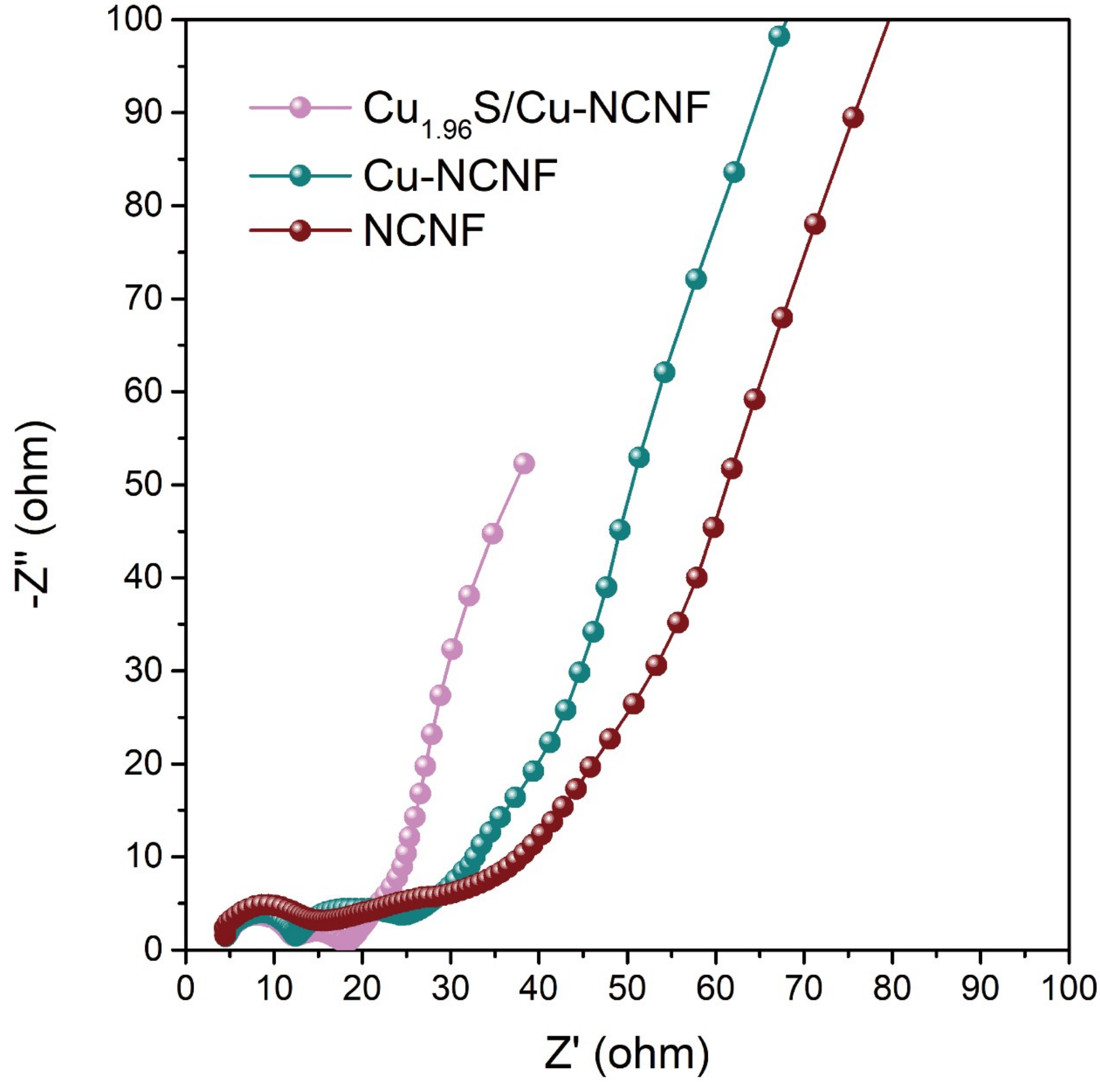

Fig. S12. Nyquist plots of $Cu_{1.96}S$/Cu-NCNF, Cu-NCNF and NCNF.

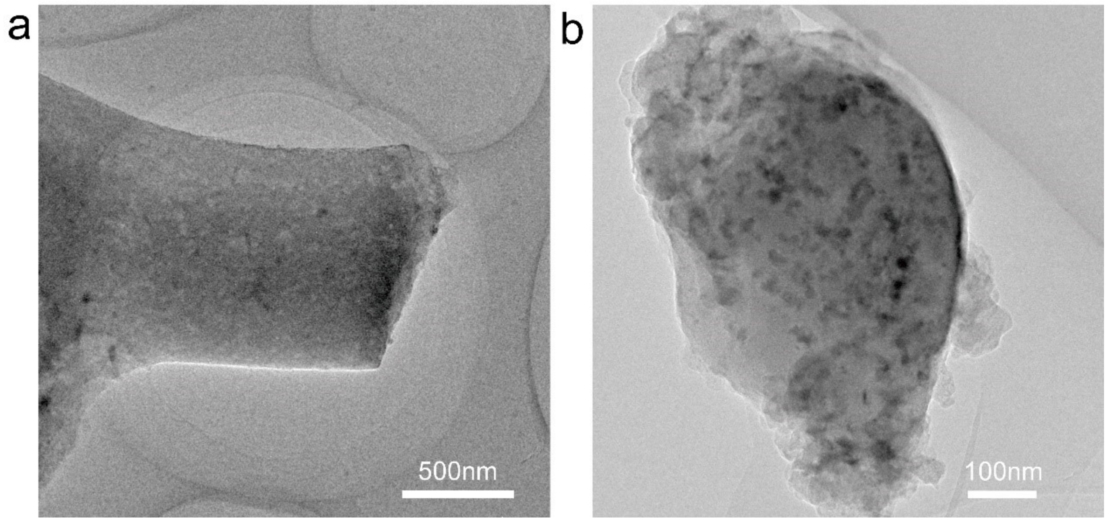

Fig. S13. TEM image of $Cu_{1.96}S$/Cu-NCNF before (a) and after (b) CO_2RR.

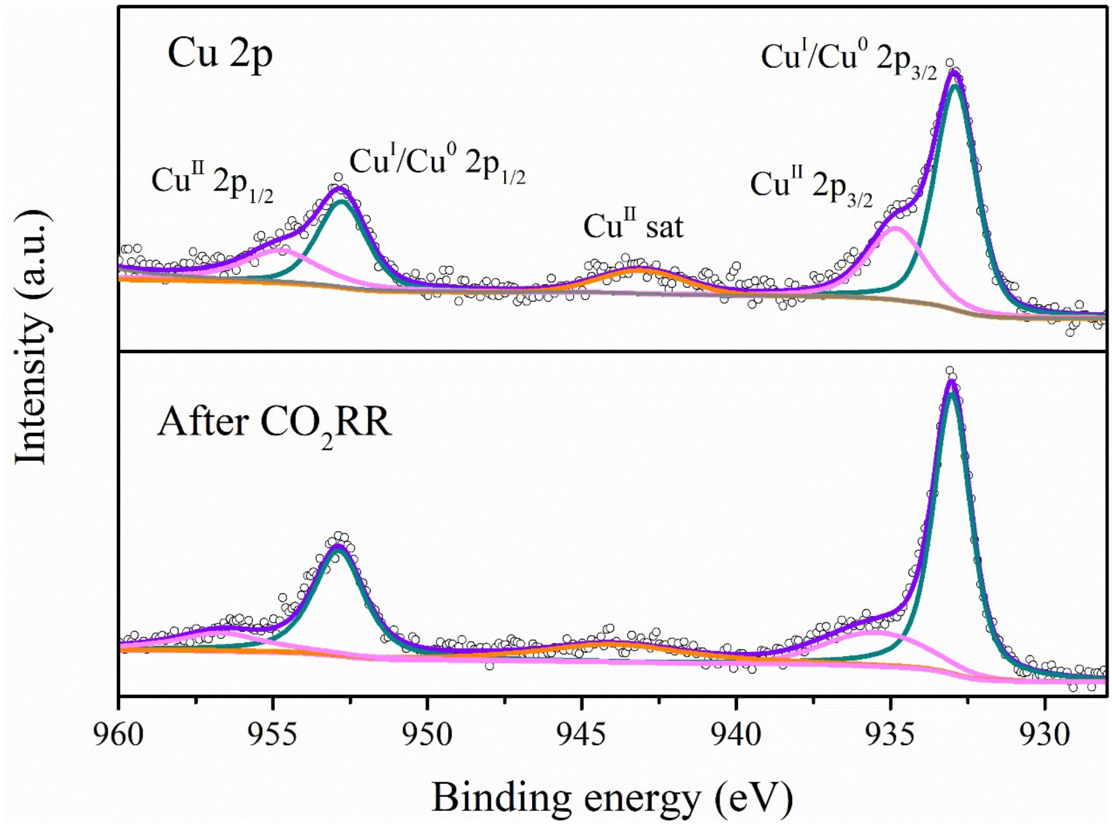

Fig. S14. XPS spectra of Cu 2p in $Cu_{1.96}S$/Cu-NCNF before and after CO_2RR.

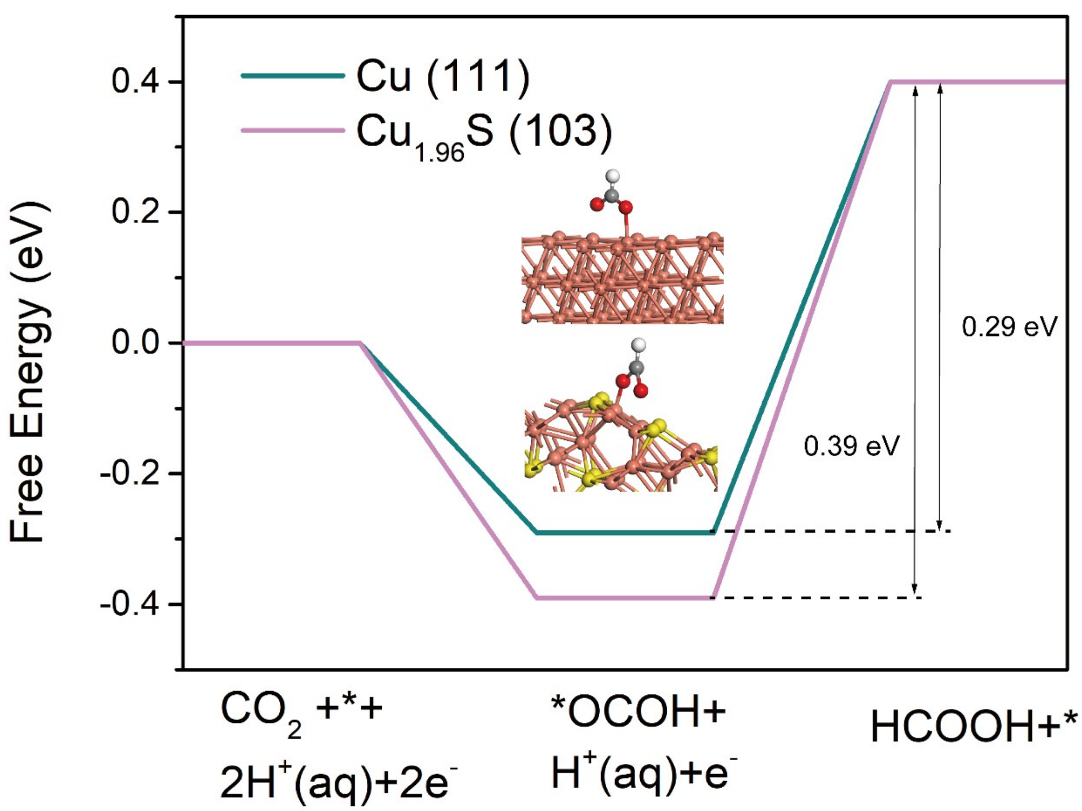

Fig. S15. Gibbs free energy diagrams for HCOOH path of Cu and $Cu_{1.96}S$.

Table S1. Summary of performances for reducing CO_2 to formate and methane on different S-modified copper.

Product	Catalysts	Potential (V vs. RHE)	Faradic efficiency (%)	Reference
CH_4	CuS nanosheet arrays	-1.1	73%	[1]
HCOOH	Sulfide-derived copper	-0.8	~50%	[2]
	Cu_2O/CuO/CuS	-0.7	84%	[3]
	CuSx	−0.6	72%	[4]
	$Cu_{1.81}S$@WMCNT-600-OD	-0.67	82%	[5]
	Sulfur-Doped Copper	-0.8	75%	[6]

Table S2. XPS Peak Table of $Cu_{1.96}S$/Cu-NCNF and Cu-NCNF.

Name	Atomic %					
	Cu 2*p*	Zn 2*p*	S 2*p*	C 1*s*	N 1*s*	O 1*s*
$Cu_{1.96}S$/Cu-NCNF	0.47	0	0.54	85.27	1.98	11.74
$Cu_{1.96}S$/Cu-NCNF-900	0.58	0.55	0.66	83.76	6.67	7.79

Table S3. Zero-pint energy and entropy contribution to the total free energy of molecules and adsorbates. All values are reported by Nørskov [7].

Species	ΔZPE (eV)	- TΔS (eV)
H_2	0.27	-0.39
H_2O	0.58	-0.65
CO_2	0.31	-0.65
CO	0.14	-0.6
*H	0.16	-0.007
*COOH	0.62	-0.18
*CO	0.19	-0.15
*OCHO	0.62	-0.23

References

1 Z. Zhao, X. Peng, X. Liu, X. Sun, J. Shi, L. Han, G. Li, J. Luo, J. Mater. Chem. A, 2017, 5, 20239-20243.

2 K. R. Phillips, Y. Katayama, J. Hwang, Y. Shao-Horn, J. Phys. Chem. Lett., 2018, 9, 4407-4412.

3 A. W. Kahsay, K. B. Ibrahim, M. C. Tsai, M. K. Birhanu, S. A. Chala, W. N. Su, B. J. Hwang, Catal. Lett., 2019, 149, 860-869.

4 J. W. Lim, W. J. Dong, J. Y. Park, D. M. Hong, J. L. Lee, ACS Appl. Mater. Interfaces, 2020, 12, 22891-22900.

5 B. Zhang, M. Wang, J. Ding, Y. Li, G. Cao, M. T. Bernards, Y. He, Y. Shi, J. CO_2 Util., 2020, 39, 101169.

6 Y. Huang, Y. Deng, A. D. Handoko, G. K. L. Goh, B. S. Yeo, ChemSusChem, 2018, 11, 320-326.

7 H. A. Hansen, J. B. Varley, A. A. Peterson, J. K. Nørskov, J. Phys. Chem. Lett., 2013, 4, 388-392.